JCI insight

RESEARCH ARTICLE

A cord blood monocyte–derived cell therapy product accelerates brain remyelination

Arjun Saha,[1] Susan Buntz,[1] Paula Scotland,[1] Li Xu,[1] Pamela Noeldner,[1] Sachit Patel,[1] Amy Wollish,[1] Aruni Gunaratne,[1] Tracy Gentry,[1] Jesse Troy,[1] Glenn K. Matsushima,[2] Joanne Kurtzberg,[1] and Andrew E. Balber[1]

[1]Robertson Clinical and Translational Cell Therapy Program, Duke Translational Medicine Institute, Duke University Medical Center, Durham, North Carolina, USA. [2]Department of Microbiology and Immunology, UNC Neuroscience Center, Integrative Program for Biological and Genome Sciences, University of North Carolina, Chapel Hill, North Carolina, USA.

Microglia and monocytes play important roles in regulating brain remyelination. We developed DUOC-01, a cell therapy product intended for treatment of demyelinating diseases, from banked human umbilical cord blood (CB) mononuclear cells. Immunodepletion and selection studies demonstrated that DUOC-01 cells are derived from CB CD14$^+$ monocytes. We compared the ability of freshly isolated CB CD14$^+$ monocytes and DUOC-01 cells to accelerate remyelination of the brains of NOD/SCID/IL2Rγ^{null} mice following cuprizone feeding–mediated demyelination. The corpus callosum of mice intracranially injected with DUOC-01 showed enhanced myelination, a higher proportion of fully myelinated axons, decreased gliosis and cellular infiltration, and more proliferating oligodendrocyte lineage cells than those of mice receiving excipient. Uncultured CB CD14$^+$ monocytes also accelerated remyelination, but to a significantly lesser extent than DUOC-01 cells. Microarray analysis, quantitative PCR studies, Western blotting, and flow cytometry demonstrated that expression of factors that promote remyelination including PDGF-AA, stem cell factor, IGF1, MMP9, MMP12, and triggering receptor expressed on myeloid cells 2 were upregulated in DUOC-01 compared to CB CD14$^+$ monocytes. Collectively, our results show that DUOC-01 accelerates brain remyelination by multiple mechanisms and could be beneficial in treating demyelinating conditions.

Introduction

Microglia play critical but incompletely understood roles in propagation and resolution of central nervous system (CNS) injuries. These cells modulate neuroinflammation, produce factors that regulate activities of astrocytes, oligodendrocytes, and neurons, and clear debris to provide an environment for oligodendrocytes to begin to remyelinate neurons (1). In mice, microglia arise from a unique pool of replicating precursors in the brain that is originally derived from the extraembryonic yolk sac early in fetal development (2). Bone marrow–derived, circulating blood monocytes constitute another potential source of infiltrating phagocytic cells that can exacerbate or ameliorate CNS damage (3). Although a pathway for circulation of monocytes between lymph and brain parenchyma has recently been described (4), large numbers of circulating monocytes do not enter the uninjured, adult mouse brain but may infiltrate the CNS following insult such as brain irradiation (5, 6), chemotherapy or injury (7), demyelinating conditions (8), or chronic stress (9, 10). In some models, these infiltrating blood monocytes may activate inflammation and participate in demyelinating events (11, 12). In others, blood monocytes may facilitate remyelination (13, 14).

Limited information is available concerning the role of human blood monocytes in the dynamics of repair of brain injury. Circulating human monocytes include subpopulations that differ in their ability to migrate to tissues, proliferate, and form inflammatory or reparative macrophages at sites of injury (15). Based on experiments in rodents, several groups have proposed that cell products composed of human monocytes could be considered as candidates for the treatment of injury-induced CNS demyelination (16, 17). CD14$^+$ monocytes present in human umbilical cord blood (CB) are among these candidates. CB

Conflict of interest: The authors have declared that no conflict of interest exists.

Submitted: February 3, 2016
Accepted: July 15, 2016
Published: August 18, 2016

Reference information:
JCI Insight. 2016;1(13):e86667.
doi:10.1172/jci.insight.86667.

mononuclear cells are protective in several in vitro culture and animal models of CNS injury (reviewed in ref. 18), and CB CD14$^+$ cells are essential for the protective ability of intravenously injected CB mononuclear cells in the rat middle cerebral artery occlusion model of stroke (19).

We have recently developed DUOC-01, a cell therapy product composed of cells with characteristics of macrophages and microglia that is intended for use in the treatment of demyelinating CNS diseases. DUOC-01 is manufactured by culturing banked CB-derived mononuclear cells (MNCs). The motile, phagocytic cells in DUOC-01 express CD45, CD11b, CD14, CD16, CD206, ionized calcium binding adaptor molecule 1 (Iba1), HLA-DR, and iNOS, secrete IL-10 and IL-6, and upregulate the secretion of cytokines in response to TNF-α and IFN-γ (20). DUOC-01 cells derived from genetically normal donors also secrete a battery of lysosomal hydrolases that are missing in children with leukodystrophies, and the initial DUOC-01 clinical trial (NCT02254863) is evaluating the safety and feasibility of treating pediatric leukodystrophy patients with the product in the setting of systemic allogeneic CB transplantation. The trial was designed so that DUOC-01, administered intrathecally, can provide cross-correcting normal enzyme to slow neurodegeneration before definitive engraftment by wild-type enzyme–producing cells from the systemic CB transplant. Studies of the biological activities of DUOC-01 suggest that it may modulate ongoing disease in other ways that could expand the potential therapeutic use of DUOC-01 to other demyelinating conditions (20).

The studies described in this report were designed to provide proof of concept for the use of DUOC-01 in treatment of demyelinating diseases that do not arise from enzyme deficiency. To accomplish this, we assessed the ability of DUOC-01 to promote remyelination of mouse brain after cuprizone-induced (CPZ-induced) demyelination, a model that has been widely used to study the mechanisms and cellular dynamics of remyelination in the corpus callosum (CC) region (21–26), and also to test the effects of various interventions, including cell therapy agents (27–30). CPZ is a Cu^{++}-chelating agent that is highly toxic to oligodendrocytes (26, 31–34), and CPZ feeding results in demyelination that can be assessed in the CC where abundant neural fiber bundles become disorganized as myelin degrades. When CPZ is removed from the diet, newly differentiated oligodendrocytes remyelinate the CC over a period of weeks. Astrocytes (35), microglia (11, 34, 36, 37), and infiltrating peripheral monocytes (11, 38, 39) have been shown to participate in the remyelination process in this model. In this study, we used the immunodeficient NOD/SCID/IL2Rγ^{null} (NSG) mice that lack functional T cells, B cells, and NK cells and readily accept human tissue grafts (40). We showed, to the best of our knowledge for the first time, that CPZ feeding in NSG mice results in reversible demyelination in the CC with a time course similar to the process in immune-competent mouse strains, and that this model can be used to assess the activity of human cell therapy products in promoting brain remyelination. Using this model, we demonstrate that the DUOC-01 cell product accelerates brain remyelination following CPZ feeding. We also show that uncultured CD14$^+$ CB cells that give rise to DUOC-01 also accelerate remyelination, but significantly less actively than DUOC-01 cells. A comparison of whole-genome expression arrays of CB CD14$^+$ monocytes and DUOC-01 revealed large differences in gene expression, and helped identify candidate molecules that may participate in remyelination. We subsequently confirmed that cells in the DUOC-01 product express and secrete several factors that promote myelination by several mechanisms.

Results

CB CD14$^+$ monocytes are essential for the production of DUOC-01 cells. To test the hypothesis that the DUOC-01 product is derived from CD14$^+$ monocytes in the CB MNC population, we simultaneously produced CD14$^+$-enriched and CD14$^+$-depleted cell populations from the same CB MNC fraction with immunomagnetic beads. Flow cytometric analysis showed that positively selected populations contained greater than 90% CD14$^+$ cells and depleted populations contained less than 2% CD14$^+$ cells. We then cultured the CD14$^+$ and CD14$^+$-depleted cell populations using the standard protocols for manufacture of DUOC-01 and compared the evolution of different cell types with cultures of CB MNCs. Six experiments were performed with fresh and 3 with cryopreserved, thawed CB units with essentially identical results. CD14$^+$-depleted cell populations did not give rise to the cell characteristic of DUOC-01. Instead, small blood cells persisted, and very few adherent cells were present. In contrast, CB CD14$^+$ monocyte populations gave rise to cultures that were morphologically indistinguishable from, and expressed surface markers characteristic of, DUOC-01. Representative results are shown in Supplemental Figure 1; supplemental material available online with this article; doi:10.1172/jci.insight.86667DS1.

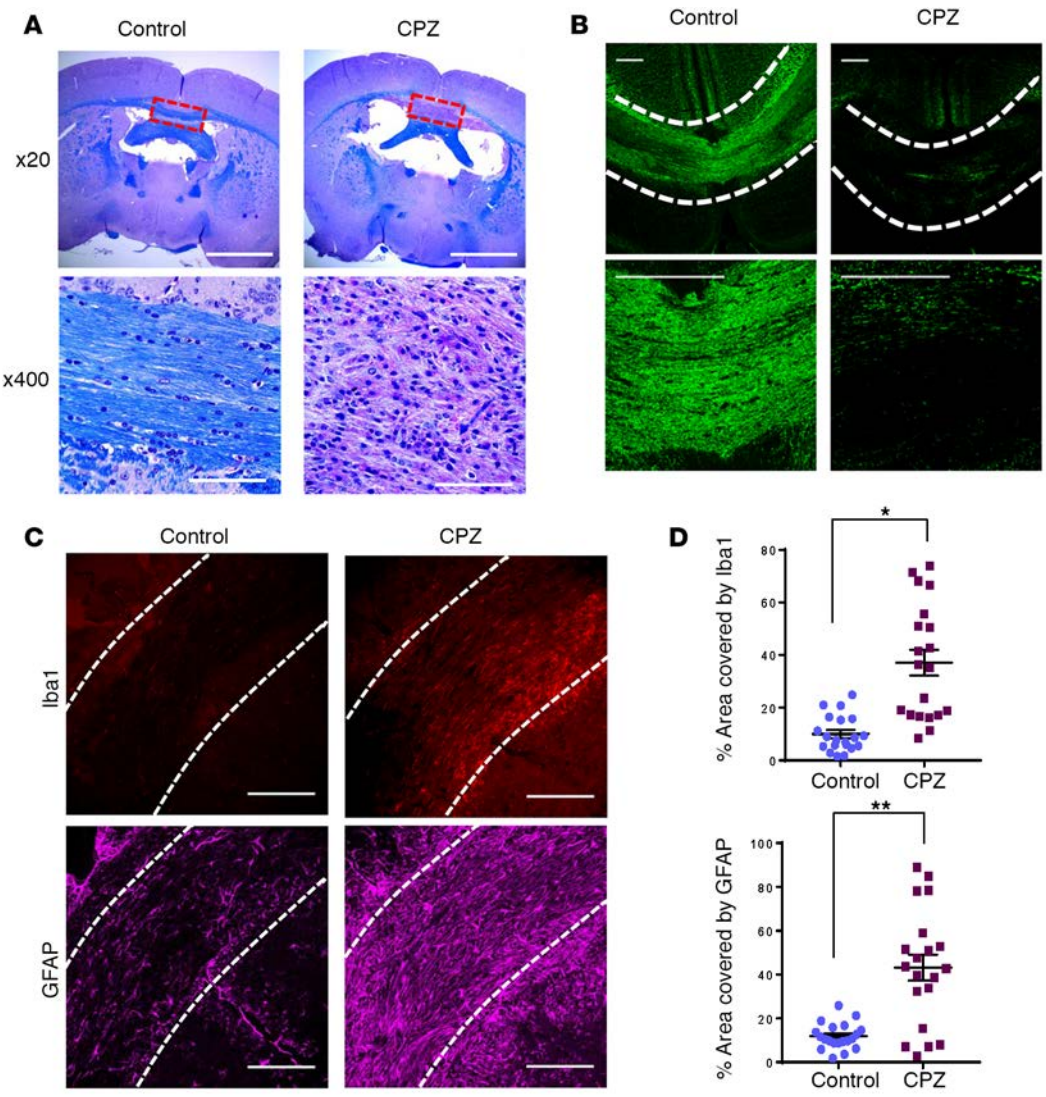

Figure 1. Severe demyelination of the midline corpus callosum (CC) area and glial infiltration of NSG mouse brain by cuprizone feeding. (**A**) LFB-PAS staining of NSG mice brain after 5 weeks of feeding with (right panel) and without (left panel) 0.2% cuprizone (CPZ). The midline CC area is shown by dotted red boxes in the top panels and then shown at higher magnification in the lower panels. Myelinated axons in the CC of mice fed normal laboratory chow are stained blue. Demyelination of the midline CC region of CPZ-treated animals is shown by the absence of the blue-colored fibers. Scale bars: 2,000 μm (×20 magnification) and 100 μm (×400 magnification). (**B**) Myelin basic protein immunostaining (green) after 5 weeks of feeding without (left panel) and with CPZ (right panel). Two different magnifications (top row is ×100 and bottom row is ×400) of the CC areas are shown. CC areas are shown by white dotted lines. (**C**) Immunostaining with microglial marker Iba1 (red, upper panels) and astrocyte marker GFAP (pink, lower panels) after 5 weeks of feeding without (left panels) and with CPZ (right panels). CC areas are shown by white dotted lines. Scale bars: 200 μm. (**D**) Quantitative analysis of area covered by Iba1-positive (upper panel) and GFAP-positive (lower panel) cells, indicative of their numbers, along the CC. Both Iba1-positive and GFAP-positive cell numbers were significantly higher in the CPZ-treated animals. $^{*}P < 0.02$, $^{**}P < 0.004$. $n = 3$ mice per group . C, control. Data are presented as the mean ± SEM.

To test the possibility that $CD34^+$ hematopoietic progenitor cells could give rise to DUOC-01 cells during manufacturing, similar experiments were carried out using immunomagnetically selected $CD34^+$ CB cells and $CD34^+$-depleted populations. In 6 experiments using fresh and 3 using cryopreserved CB, $CD34^+$cells survived poorly, and no cells resembling DUOC-01 arose in culture (data not shown). In contrast, $CD34^+$-depleted cell populations gave rise to normal numbers of DUOC-01 cells.

Since the $CD14^+$ cell population is essential for the generation of the DUOC-01 cell product, we proceeded to compare the ability of freshly isolated CB $CD14^+$ monocytes and 21 day–cultured DUOC-01 cell products to influence remyelination of the CC region in CPZ-fed mice. To increase survival of human cells

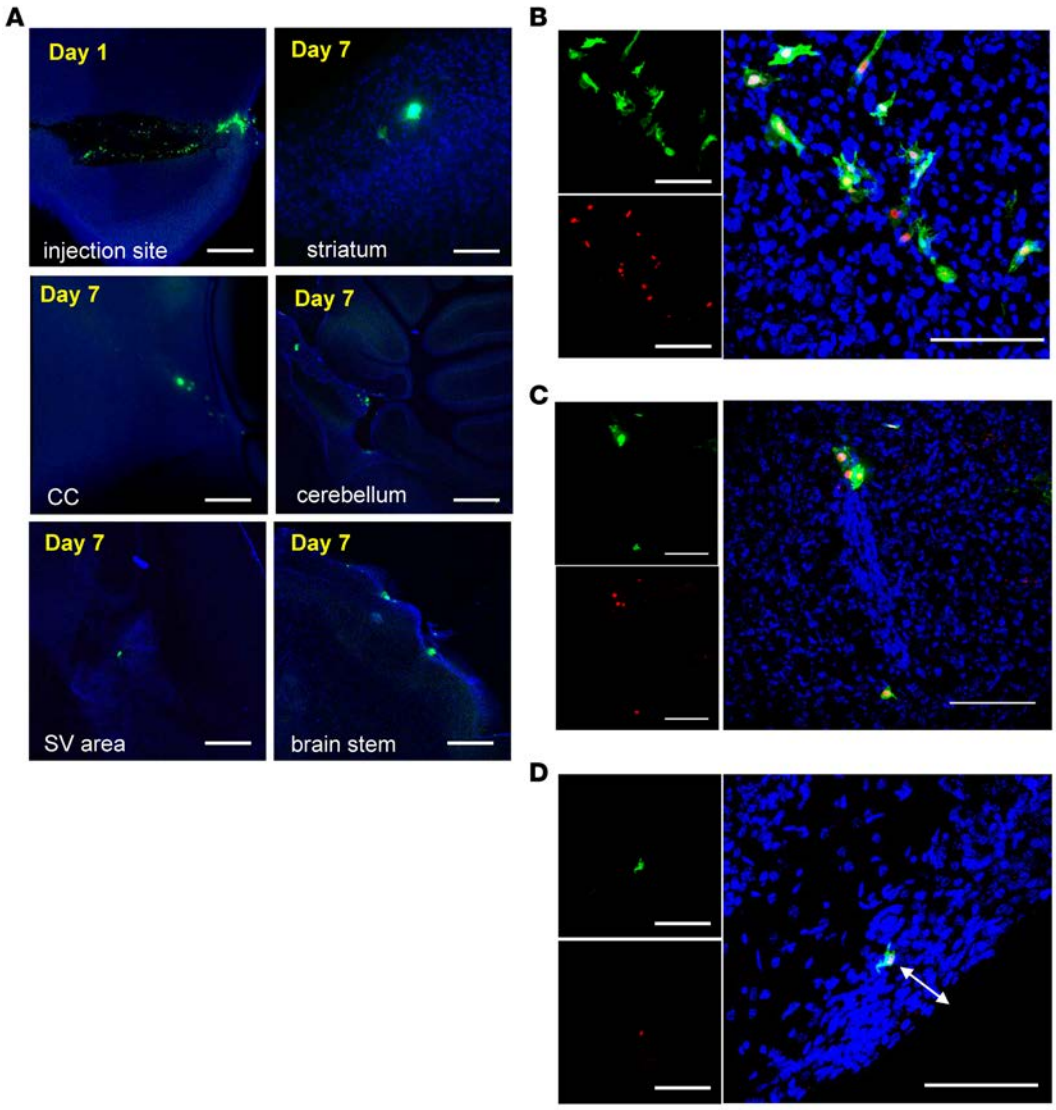

Figure 2. Some DUOC-01 cells disseminated from the injection site and persisted in the brain for up to 1 week after intracranial injection. Cuprizone-fed (CPZ-fed) mice were stereotactically injected with CFSE-labeled DUOC-01 cells. All cell nuclei were stained with DAPI (blue). (**A**) CFSE-labeled (green) DUOC-01 cells were found in numerous parts of the brain including the injection site. Scale bars: 200 μm. CC, corpus callosum; SV, subventricular. (**B**) Representative images of CFSE-positive (green) and human nuclei (HuN, red)-positive cells in the brain at the injection site 4 days after injection. Upper left panel is CFSE (green) channel only, lower left panel is HuN (red) channel only, right panel is merge of CFSE, HuN, and DAPI channels. (**C**) Upper left panel is CFSE channel only, lower left panel is HuN channel only, right panel is merge of CFSE, HuN, and DAPI channels showing presence of DUOC-01 cells 7 days after injection at the CC. (**D**) Upper left panel is CFSE channel only, lower left panel is HuN channel only, right panel is merge of CFSE, HuN, and DAPI channels showing presence of DUOC-01 cells deep (white arrow) into the brain parenchyma. Scale bars (**B**–**D**): 100 μm.

used for treatment in this xenogeneic model, we chose to use the immune-incompetent NSG mice for our CPZ-mediated demyelination and remyelination studies.

CC region of NSG mice was severely demyelinated and disorganized following CPZ feeding. Because different mouse strains may respond to CPZ feeding in significantly different ways (23) and because NSG mice have not previously been used in this model, we first studied the process of demyelination and remyelination of the CC in NSG animals in the absence of cell therapy. Very similar results were obtained in each of 4 experiments. Similar to C57BL/6 mice fed 0.2% CPZ (38) for 5 weeks, NSG mice weighed 12%–16% less than mice on normal diets (Supplemental Figure 2) and gained weight similarly to the control strain when they were returned to the normal laboratory chow after 5 weeks of CPZ feeding. Neither CPZ feeding nor injection of any of the 3 cell populations induced any obvious changes in overall behavior or general health of the animals.

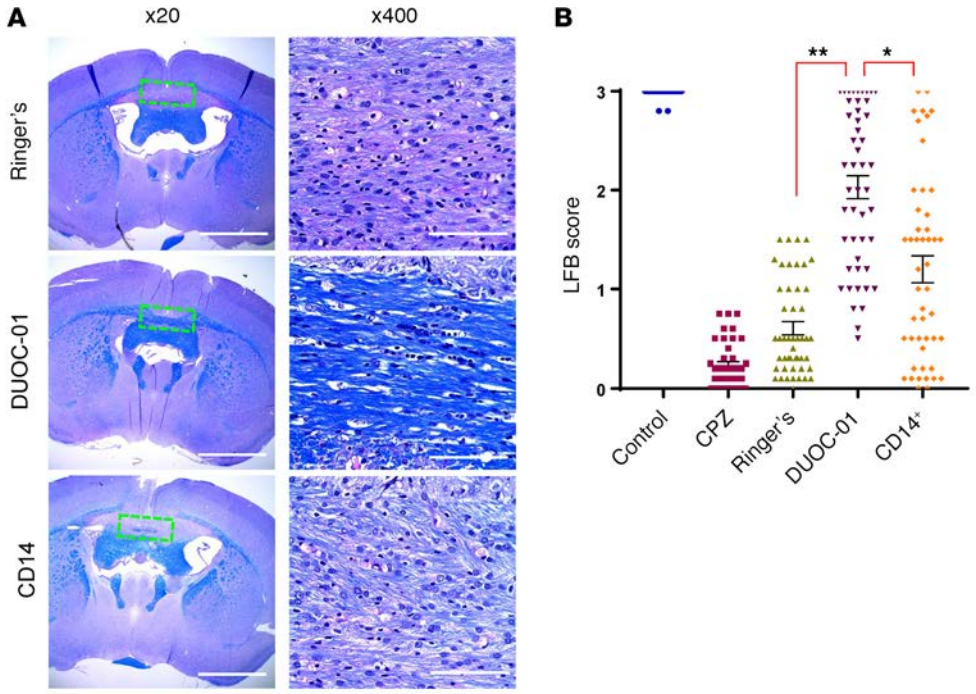

Figure 3. LFB-PAS staining analysis of effect of DUOC-01 treatment on remyelination following cessation of cuprizone (CPZ) treatment. (**A**) LFB-PAS staining 1 week after intracranial injection of CD14$^+$ monocytes (lower panels), DUOC-1 cells (middle panels), or Ringer's solution (upper panels) in CPZ-fed NSG mice. Midline corpus callosum (CC) area is shown by dotted green line. Scale bars: 2,000 μm (×20 magnification) and 100 μm (×400 magnification). (**B**) Myelination score based on LFB-PAS staining of mice fed normal chow (control) or CPZ for 5 weeks 1 week after treatment of CPZ-treated mice with CD14$^+$ monocytes, DUOC-01 cells, or Ringer's. DUOC-01 treatment for 1 week significantly increased the myelination in the CC area compared to Ringer's-injected controls. $^{**}P < 5.962 \times 10^{-5}$ for this study. The CD14$^+$ cell–treated sample showed an increased amount of remyelination compared to the Ringer's-treated group, but it was significantly less than the DUOC-01–treated group. $^{*}P < 0.003875$. Data are presented as the mean ± SEM. Statistical comparisons were performed using the Wilcoxon rank-sum test for clustered data using the *clusrank* package in R.

After 5 weeks of CPZ feeding, the extent of myelination in the CC was examined by staining coronal brain sections with Luxol fast blue-periodic acid Schiff (LFB-PAS). The CC region of NSG mice was severely demyelinated, with gliosis following CPZ feeding compared with control mice on standard chow (Figure 1A). Figure 1A also shows that peripheral regions of the CC were less affected. Thus, NSG mice exposed to CPZ demyelinate in the CC, similarly to what has been reported for C57BL/6 mice (41).

Immunohistochemical analysis confirmed morphological and cellular effects of CPZ feeding. The midline CC region of the brains of mice fed CPZ for 5 weeks showed very little or no staining for myelin basic protein (MBP) compared with uniform MBP staining in control animals (Figure 1B). Astrocytes positive for glial fibrillary acidic protein (GFAP) and microglia positive for Iba1 were much more profuse in the CC region of CPZ-fed animals than those of controls (Figure 1C), indicative of severe gliosis. Expression of both GFAP and Iba1 per unit surface area in the CC region was significantly greater in the CPZ-treated mice than in the control mice (Figure 1D).

Electron microscopic analysis of the CC also confirmed that CPZ caused severe demyelination and showed additional disruptions of axonal structure in the region (Supplemental Figure 3A). Spontaneous remyelination kinetics of NSG mouse brains after CPZ withdrawal was evaluated by LFB-PAS staining. We found that, 1 week after CPZ withdrawal, most of the midline CC area of NSG mouse brains remained severely demyelinated (Supplemental Figure 4). However, 2 weeks after CPZ withdrawal, the midline CC area of the brain was significantly remyelinated (Supplemental Figure 4). Thus, the effects of CPZ feeding on the CC region of NSG mice are generally similar to the effects in the more commonly used C57BL/6 mouse strain, and we used this model to explore the effects of DUOC-01 treatment on the kinetics of remyelination once CPZ feeding was terminated.

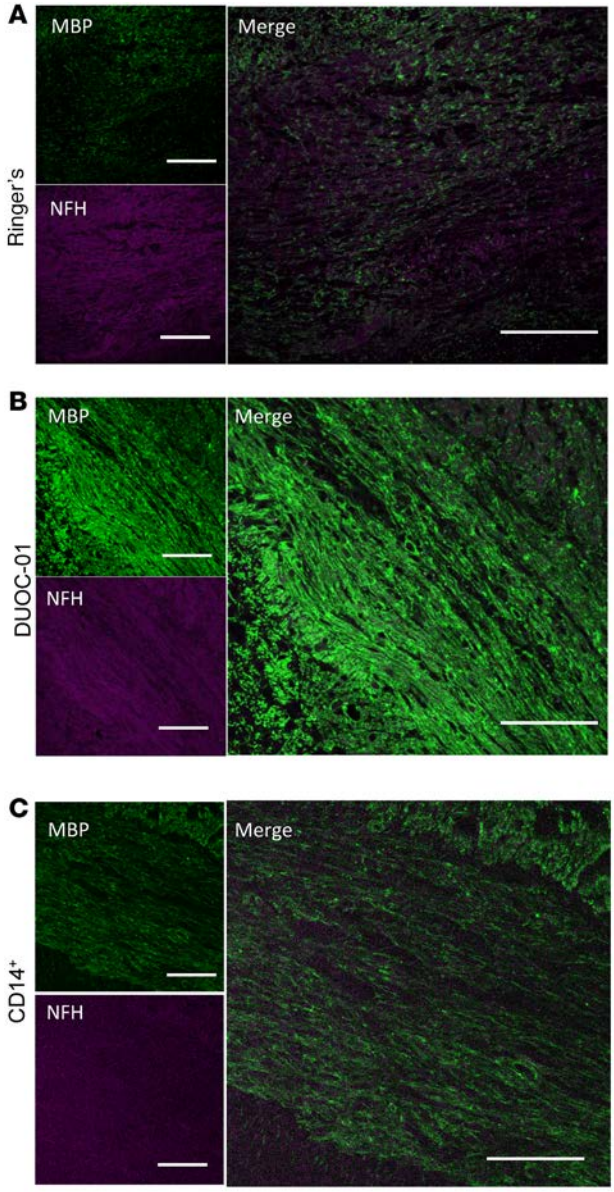

Figure 4. Immunostaining analysis of the effect of DUOC-01 treatment on remyelination following cessation of cuprizone (CPZ) treatment. In all images, myelin basic protein (MBP) staining is shown in green. (**A**) Representative ×400 laser confocal images of sections of the corpus callosum (CC) area of CPZ-fed mice immunostained with antibodies against MBP (green) and neurofilament-H (NFH, purple), 1 week after treatment with Ringer's solution (**A**), DUOC-01 (**B**), or $CD14^+$ (**C**). Upper left panels show MBP (green channel), lower left panels show NFH (purple channel), and right panels show enlarged merge images of MBP and NFH channels. Scale bars: 100 μm.

DUOC-01 cells disseminated from the injection site and persisted in the brain for up to 1 week after intracranial injection. To trace human cells in the brain following stereotactic injection in the midline CC area, NSG mice that had been fed CPZ for 5 weeks were injected intracranially with 1.0×10^5 CFSE-labeled DUOC-01 cells. CFSE stains the cells fluorescent green, and the dye is stable for weeks in vivo (42). CFSE-labeled cells were found at the injection site as well as in the striatum, CC, cerebellum, brain stem, and subventricular area up to 7 days after injection (Figure 2A). To further confirm that the CFSE-positive cells observed in brain sections were injected DUOC-01 cells, we performed immunostaining with an antibody that specifically detects human nuclei (anti-HuN). Mouse cells in the brain sections were not positive for this anti-HuN antibody. In contrast, the CFSE-positive cells costained with anti-HuN (Figure 2B), confirming that the CFSE-stained cells were not mouse brain cells that might have taken up CFSE released by DUOC-01 or stained human cell debris. CSFE- and HuN-costained DUOC-01 cells were detected deep in the brain parenchyma and as far from the CC injection site as the frontal cortex, and persisted for up to 1 week until assessment of myelination (Figure 2C). We also found CFSE-stained $CD14^+$ cells in various parts of the brain even after 7 days after intracranial injections (Supplemental Figure 5). Thus, DUOC-01 cells disseminated bilaterally from the injection site and persisted in the brain during the 1-week period between cell injection and harvesting brains for assessment of myelination status.

DUOC-01 treatment accelerates remyelination after CPZ feeding in the CC region of NSG mice. As noted above, LFB-PAS staining showed that NSG mice spontaneously remyelinated the CC region during 2 weeks following termination of CPZ feeding (Supplemental Figure 4). In all 4 experiments, the CC of CPZ-fed mice treated with Ringer's remained severely demyelinated 1 week after diet change and injection (Figure 3A). In contrast, LFB-PAS staining showed extensive myelin fiber formation in the CC 1 week after treatment with DUOC-01 (Figure 3A). Myelination scores of the CC of DUOC-01–treated mice were significantly higher than those of the Ringer's-injected group (Figure 3B). $CD14^+$ cell–treated mice also showed an increased amount of remyelination compared with the Ringer's control group, but significantly less than the DUOC-01–treated group (Figure 3, A and B). We examined the effects of DUOC-01 treatment in remyelination in more detail.

Immunohistochemical analysis with an anti-MBP antibody confirmed that DUOC-01–treated mice remyelinated more extensively than Ringer's control animals during the week after diet change and treatment (Figure 4A). Analysis of higher magnification confocal images revealed a higher density and level of organization of MBP-containing fibers in the CC of DUOC-01–treated mice (Figure 4B), and MBP appeared to colocalize with neurofilament-H (NFH) (Figure 4B), indicative of myelin wrapping along the axonal fibers.

Electron microscopic analysis revealed that the newly synthesized myelin detected by immunohistochemistry in the CC of DUOC-01–treated mice was organized into myelin sheaths on axons (Figure 5). Morphometric analysis revealed that the CC of DUOC-01–treated mice had significantly more myelinated axons than the CC of animals treated with Ringer's (Figure 6A). To further assess

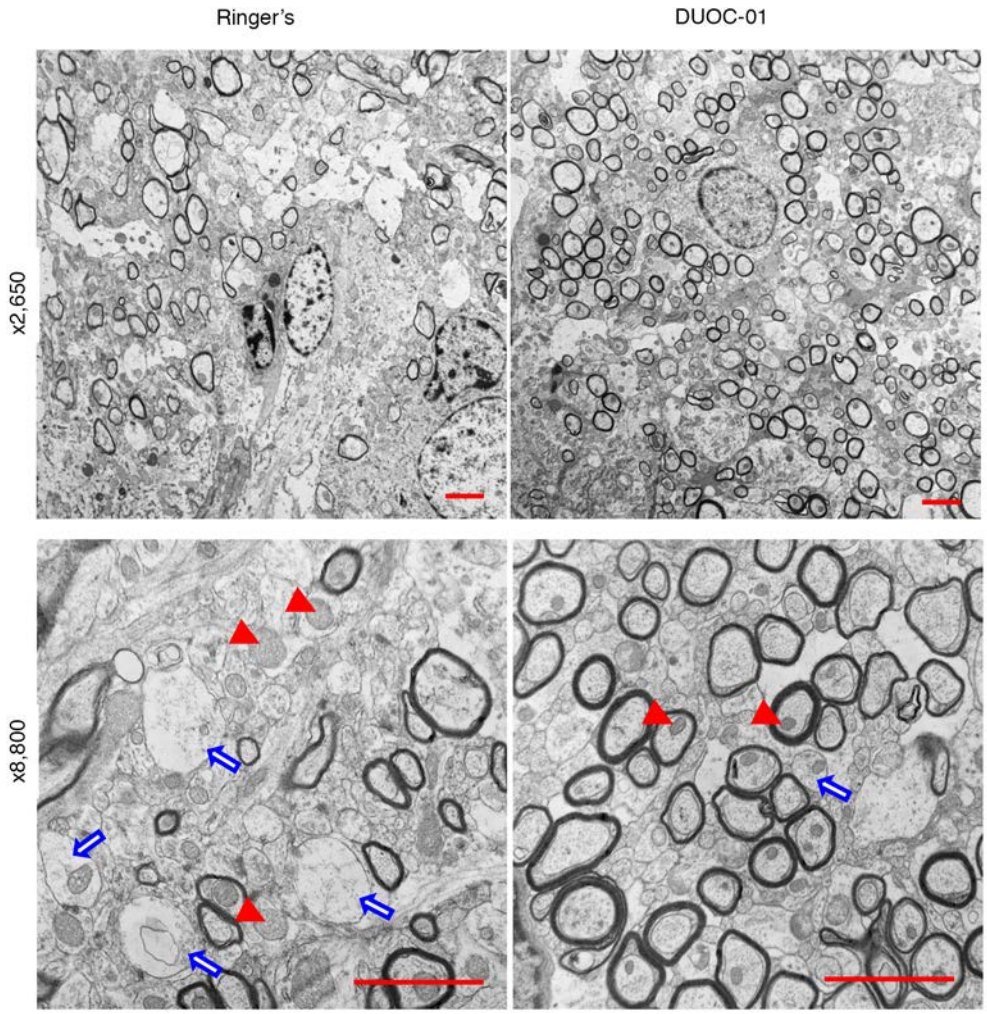

Figure 5. Electron microscopic analysis of remyelination status upon DUOC-01 treatment. Representative ×2,650 (upper panels) and ×8,800 (lower panels) electron micrographs of corpus callosum region of cuprizone-fed mice 1 week after injection of Ringer's solution (left panels) or DUOC-01 cells (right panels). Blue arrows indicate unmyelinated axons. Red arrowheads indicate mitochondria; enlarged mitochondria are clearly visible in the Ringer's-treated group. Scale bars: 2.0 μm.

the organization of the myelin sheath, we counted the number of turns of myelin sheath wrapped around the axons. The DUOC-01–treated group had approximately 2 additional turns of myelin sheath per axon compared with the control group (Figure 6B). We also found that the g-ratio (ratio of the inner axonal diameter to the total outer [including myelin wrap] diameter) value was lower in DUOC-01–treated compared with the Ringer's-treated mice, indicating increased myelin thickness in DUOC-01–treated mice (Figure 6C). Supplemental Figure 6A shows that axonal diameters displayed a similar distribution of higher and lower g-ratios across various axon diameters both in Ringer's- and DUOC-01–treated groups. We also explored whether cell treatment had an impact on axonal density in the CC area. Axonal density, measured as the number of axons present per microscopic field (×8,800 magnification) of electron micrographs, was not significantly different ($P < 0.075$) in the DUOC-01–treated and the Ringer's-treated samples (Supplemental Figure 6B). Taken together, these data show that relative to Ringer's treatment, administration of DUOC-01 cells increased the number of remyelinated axons and augmented the myelin thickness and organization in the CC in the 7 days following treatment.

Morphometric analysis also showed that treatment with DUOC-01 accelerated the reversal of megamitochondria formation (Figure 5 and Supplemental Figure 3B). One week after DUOC-01 cell treatment, the average size of mitochondria in the brain cells of Ringer's-treated mice was significantly larger

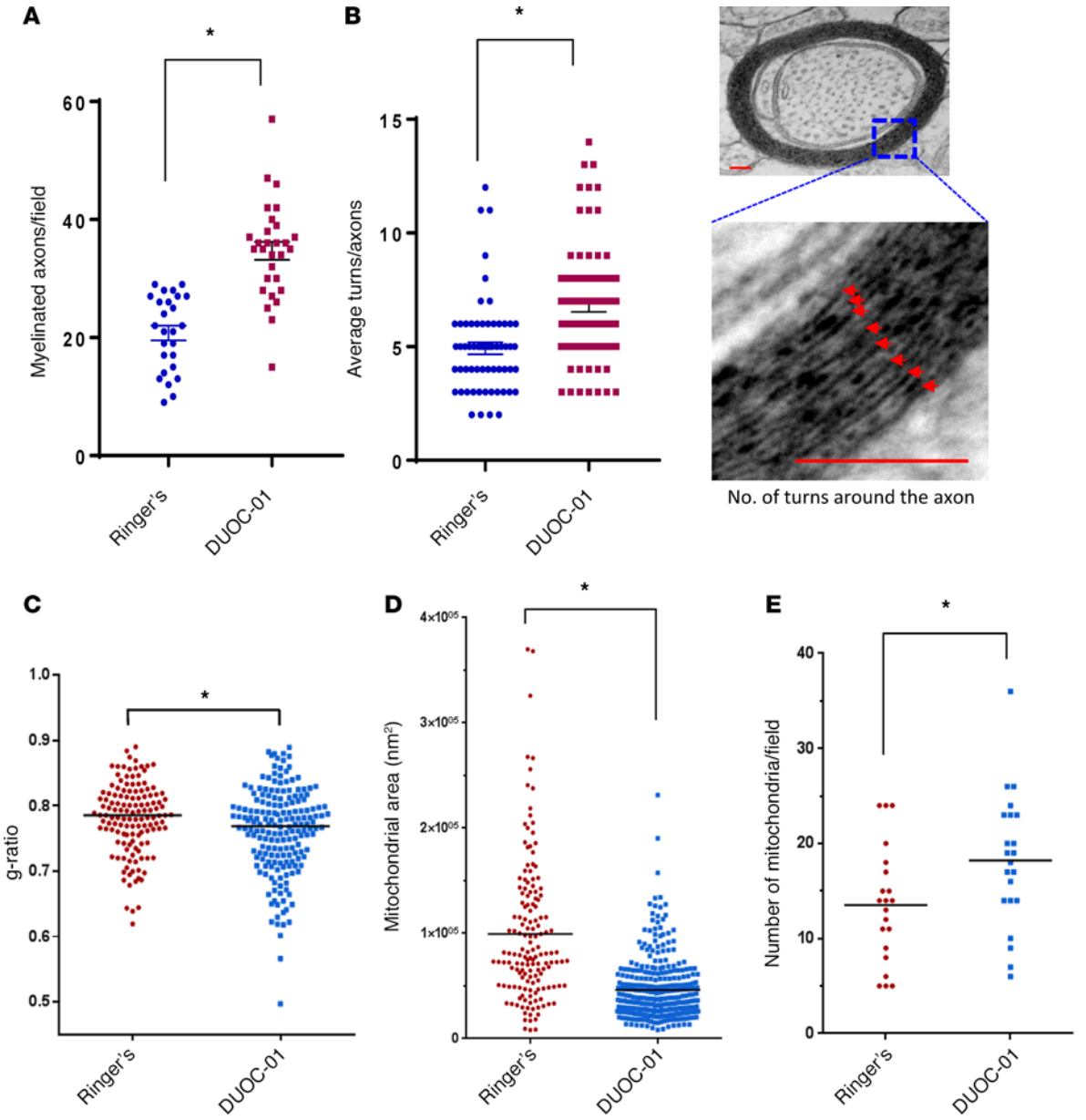

Figure 6. Morphometric analysis of electron micrographs of corpus callosum regions of DUOC-01– and Ringer's-treated mice. (**A**) Number of myelinated axons present per ×8,800 electron microscopy field. Data are presented as the mean ± SEM showing all the data points. *$P \leq 4.29 \times 10^{-9}$. (**B**) Average number of turns of myelin sheath around axons, with right panels showing a representative electron micrograph of the myelin turns in an axon. *$P \leq 3.4 \times 10^{-6}$. Scale bars: 100 nm. (**C**) Scatter plot of g-ratios, showing axonal measurements from 3 different animals in each group. Horizontal lines indicate mean g-ratios. $P \leq 0.014$. (**D**) Average size of mitochondria (area in nm^2). Mean difference is significant between DUOC-01 and Ringer's groups. *$P \leq 9.3 \times 10^{-5}$. (**E**) Average number of mitochondria per ×8,800 field. The mean difference is significant between DUOC-01 and Ringer's groups. *$P \leq 0.02$. Each column represents the value of measurements from 3 different animals. Error bars indicate the SEM. Statistical comparisons were performed using an unpaired 2-tailed Student's *t* test.

than in cells of the DUOC-01–treated group (Figure 6D). Electron micrographs (Supplemental Figure 3B) show that mitochondria of DUOC-01–treated brains were similar in size to those in unmyelinated control brains. In the Ringer's-treated group, enlarged mitochondria were present in both axons as well as in other cells, possibly in oligodendrocytes (Supplemental Figure 3B). Brains from DUOC-01–treated mice had a greater number of mitochondria per electron microscopic field than brains from Ringer's-treated animals (Figure 6E). This reduction in mitochondrial size coupled with the observed increase in mega-mitochondria formation and larger numbers of mitochondria suggests that DUOC-01 cells helped restore mitochondrial activity during remyelination.

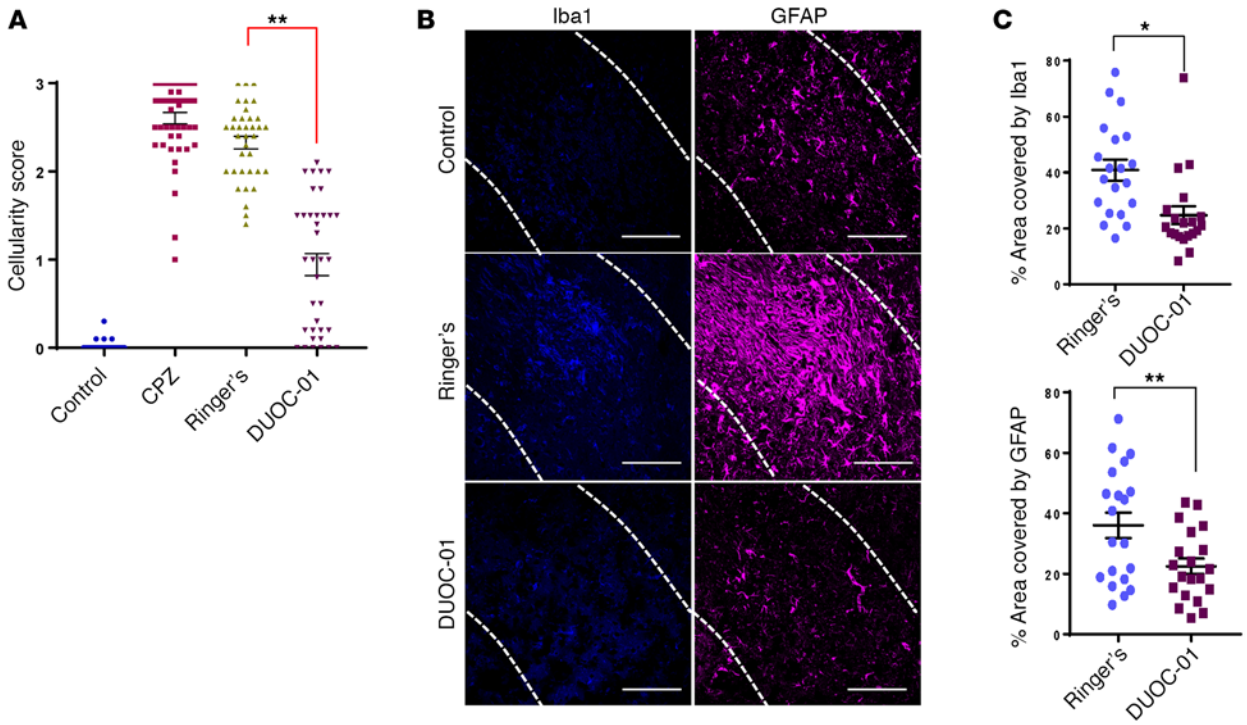

Figure 7. DUOC-01 cell treatment reduces severe astrogliosis and microglial infiltration. (**A**) A quantitative cellularity scoring of LFB-stained brain slices on a scale of 0 to 3. $^{**}P \leq 7.618 \times 10^{-5}$, $n \geq 5$. Control, not cuprizone fed; CPZ, cuprizone fed; Ringer's, 1 week after Ringer's injection; DUOC-01, 1 week after DUOC-01 injection. Data are presented as the mean ± SEM showing each data point. Statistical comparisons were performed using the Wilcoxon rank-sum test for clustered data using the *clusrank* package in R. (**B**) Cellularity status by immunostaining using astrocyte-specific (GFAP, right panels) and microglia-specific (Iba1, left panels) markers. Midline corpus callosum (CC) areas are shown in dotted line. Scale bars: 100 μm. (**C**) Quantitative analysis of area covered by Iba1-positive (upper panel) and GFAP-positive (lower panel) cells, indicative of their numbers, along the CC. Both the numbers of Iba1-positive (microglia) and GFAP-positive (astrocytes) cells were significantly lower in the DUOC-01–treated mice. $^{*}P < 0.002$; $^{**}P < 0.01$. $n = 3$ mice per group. Areas covered by each channel (either GFAP or Iba1) per microscopic field were quantified by ImageJ software. Data are presented as the mean ± SEM. Statistical comparisons were performed using an unpaired 2-tailed Student's *t* test.

Cellularity scoring of LFB-PAS stains of CC sections showed that DUOC-01 treatment also significantly reduced cellular accumulation and gliosis in the CC region 1 week following diet change (Figure 7A). Reduced glial accumulation was also evident in brain sections stained with antibodies against GFAP to detect astrocytes and Iba1 to detect microglia (Figure 7B). We performed quantitative analysis of areas covered by Iba1- and GFAP-positive cells, indicative of their numbers, along the CC. Both the numbers of Iba1-positive (microglia) and GFAP-positive (astrocytes) cells were significantly lower in the CC area of the DUOC-01–treated animal brains (Figure 7C). The cellularity score also was decreased in the $CD14^+$ cell–injected group (Supplemental Figure 7) compared to the Ringer's-injected control, but not as markedly as the DUOC-01–treated group.

DUOC-01 cell treatment promotes oligodendrocyte progenitor proliferation. We next determined whether DUOC-01 treatment increased the number of proliferating oligodendrocyte progenitor cells in the CC area following cessation of CPZ feeding (Figure 8). In adult brains, the oligodendrocyte lineage transcription factor 2 (Olig2) is present in the nuclei of oligodendrocyte progenitors and mature oligodendrocytes (43, 44). Ki67 is only present in proliferating cells (45). Thus, we used the combination of anti-Olig2 and anti-Ki67 antibodies to detect newly generated cells in the oligodendrocyte lineage. The number of proliferating $Olig2^+Ki67^+$ oligodendrocytes (Figure 8B) present in the CC region was significantly higher in brain sections from DUOC-01–treated animals than in controls that did not receive cell therapy. There was no significant increase in the number of proliferating $Olig2^+Ki67^+$ oligodendrocytes in CB $CD14^+$–treated brains as compared with the Ringer's-injected group (data not shown). Thus, DUOC-01 treatment promotes oligodendrogenesis, which in turn could facilitate remyelination.

Identification of gene products expressed by DUOC-01 that may promote remyelination. We used whole-genome expression microarrays to identify candidate DUOC-01 genes that may participate in acceleration of remyelination of the CC following CPZ feeding. Since DUOC-01 cells promote remyelination much

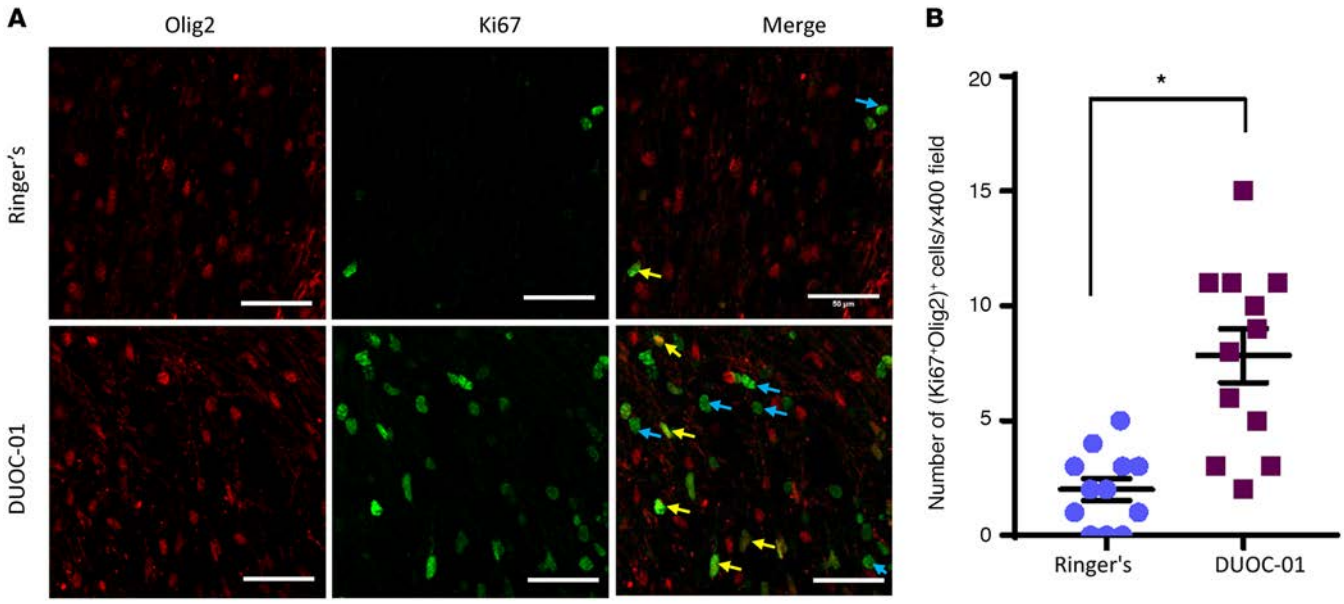

Figure 8. DUOC-01 treatment promotes oligodendrocyte proliferation. (**A**) Representative image of corpus callosum area of brains of cuprizone-fed mice treated with DUOC-01 cells (lower panels) or Ringer's solution (upper panels) stained with antibodies against Olig2 and Ki67. Yellow arrows indicate nuclei positive for both Olig2 and Ki67, blue arrows indicate only Ki67-positive nuclei. Scale bars: 50 μm. (**B**) Average number of $Olig2^+Ki67^+$ cells (indicating proliferating oligodendrocytes) present per ×400 microscopic field were significantly higher in DUOC-01–treated samples compared to the Ringer's control. $^*P < 0.01$. Statistical comparisons were performed using an unpaired 2-tailed Student's *t* test.

more robustly than CB $CD14^+$ monocytes, our initial strategy was to identify differentially expressed transcripts that were more abundant in DUOC-01 than in CB $CD14^+$ monocytes. We performed whole-genome microarray analysis on 4 highly purified, flow cytometry–sorted, CB $CD14^+$ monocytes and 3 DUOC-01 cell products. Complete expression data have been deposited in the NCBI's Gene Expression Omnibus (GEO GSE76803).

We used stringent MAS5 analysis to identify expressed genes. In order for a transcript corresponding to a probe to be scored as "present," we required that all 4 CB $CD14^+$ cell samples or all 3 DUOC-01 samples on the chip showed expression with a specific probe set (Supplemental File 1). A Venn diagram displaying the findings from microarray analysis showing the number of genes only expressed in purified fresh $CD14^+$ or DUOC-01 cells as well as genes expressed by both cell types is shown in Figure 9A. For less stringent analysis, transcripts that were not detected in at least 1 sample, but detected in others were scored as "mixed," and transcripts absent in all samples were scored as "absent." The 2 cell populations differed considerably in gene expression. Thus, 1,184 probe sets detected transcripts in all DUOC-01 samples that were absent in all CB $CD14^+$ monocyte samples and, conversely, 1,017 transcripts were present in all CB $CD14^+$ monocytes and absent in all DUOC-01 samples. In addition, 3,189 probe sets detected transcripts in 1 or 2 of the 3 DUOC-01 lots but none of the 4 CB $CD14^+$ preparations. Conversely, 3,496 probes detected transcripts in 1, 2, or 3 of the 4 CB $CD14^+$ preparations but none of the DUOC-01 lots. Additional differences in expression were observed when requirements were less stringent.

We also analyzed quantitative changes in the level of expression of transcripts expressed by both cell populations when CB $CD14^+$ monocytes differentiated into DUOC-01 (Supplemental File 2). Lists of expressed genes were generated using the Partek software suite, with stringency set such that a probe was scored as expressed if 3 or 4 of the CB $CD14^+$ cell samples showed expression or 2 or 3 of the DUOC-01 samples showed expression. ANOVA was performed on robust multiarray average–normalized (RMA-normalized) expression levels, and all genes that showed greater than 2-fold differences in expression between the 2 groups were identified and selected for further analysis. Altogether, 8,566 probes detected transcripts that were significantly ($P < 0.05$) expressed at least 2-fold differently between the 2 populations. Of these, 3,585 probes detected transcripts expressed at higher levels in CB $CD14^+$ monocytes, and 4,979 probes detected transcripts more highly expressed in DUOC-01. The volcano plot in Figure 9B graphically represents the marked difference in the gene expression pattern between the 2 cell types. Tabular representation of

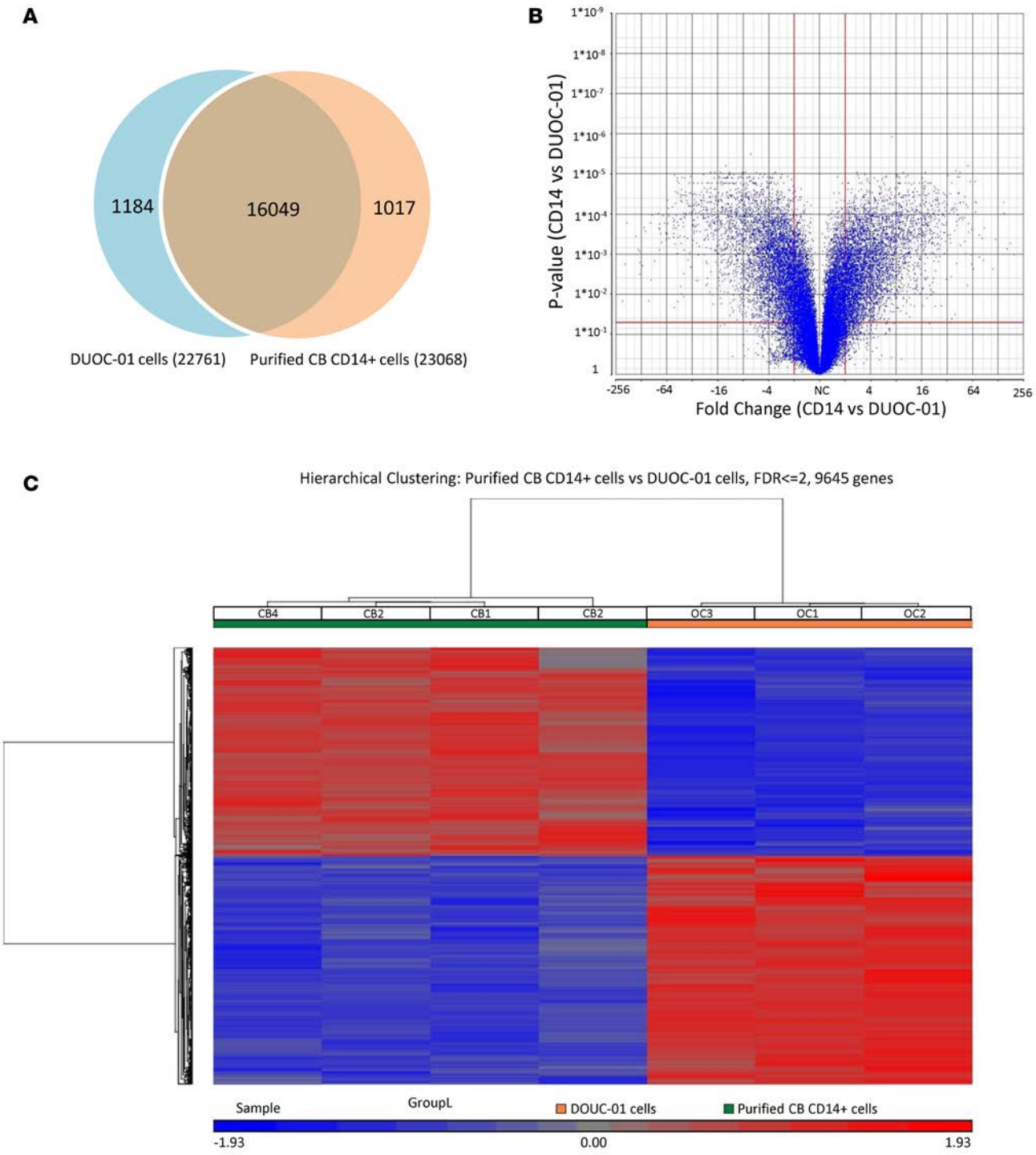

Figure 9. Comparative whole-transcriptome analysis of CD14 and DUOC-01 cells. (**A**) Venn diagram displaying the findings from microarray analysis showing the number of genes differentially expressed in purified fresh CD14$^+$ (n = 4) and DUOC-01 (n = 3) cells as well as genes expressed by both cell types. MAS5-normalized data were used to filter out expressed/nonexpressed genes. The figure represents the most stringent analysis; to be scored as expressed, the transcript had to be detected above background in all samples of a given cell type analyzed. See the text for expression figures at different stringencies. (**B**) Volcano plot depiction of findings from microarray analysis showing the genes differentially expressed in purified fresh CD14$^+$ and DUOC-01 cells. The $\log_{10}$ of Bonferroni-Hochberg–corrected P values in ANOVA (y axis) is plotted against the of fold change between 2 groups (x axis). Red lines delineate the cutoffs for genes significantly ($P < 0.05$) downregulated (left) or upregulated (right) in DUOC-01 cells. Each data point represents 1 gene probe set. (**C**) Heat maps showing differentially expressed genes. Up- and downregulated genes are displayed in red and blue, respectively. There were 9,645 genes that are differentially expressed at a magnitude of at least 2-fold.

Table 1. Quantitative PCR determination of abundance of transcripts of factors that promote oligodendrogenesis and myelination in DUOC-01 and CB CD14⁺ monocytes.

Gene name	Fold change (Mean ± SEM, $n > 3$)	*P* value
PDGFA	32.3 ± 8.3	≤0.01
KITLG/SCF	26.7 ± 4.8	≤0.033
IGF1	799 ± 294	≤0.05
MMP9	632 ± 109	≤0.002
MMP12	2057 ± 460	≤0.006
TREM2	1634 ± 368	≤0.011

Pearson's correlation coefficients among the samples (Supplemental Figure 8) showed a lower correlation (0.87–0.90) among the CB CD14⁺ and DUOC-01 groups, although the correlation coefficient was much higher (0.97–0.99) between the samples within the same group. Differentially expressed transcripts are listed in GEO GSE76803. The heat map presented in Figure 9C also demonstrates that DUOC-01 and CB CD14⁺ cells fall into discrete populations defined by a large number of differentially expressed transcripts.

To annotate the function of genes that were differentially expressed, we eliminated uncharacterized transcripts, pseudogenes, and non–protein-coding transcripts from further analysis. The resulting gene lists were examined using the tools aggregated at the DAVID website (46, 47). Supplemental File 2 shows the functional cluster analysis for the genes that are more highly expressed in DUOC-01 cells than CB CD14⁺ monocytes. This list is enriched for genes involved in all aspects of cell division and mitosis. Pathway analysis also shows an abundance of genes involved in cell division and in lysosomal activity and trafficking of intracellular vesicles. Of interest, genes encoding factors previously shown to be secreted and/or increased (e.g., IL-10, TGF-β, and galactocerebrosidase [GALC]) during manufacturing of DUOC-01 (20), were identified in the DUOC-01 upregulated gene list. In addition, transcripts for several other lysosomal enzymes that are secreted by DUOC-01 (20) are more abundant in the cell product than in CB CD14⁺ cells, and pathway analysis shows a very high probability of enrichment for genes encoding proteins in the lysosomal lumen in DUOC-01 (Supplemental File 2). A variety of transcripts that can influence myelination are highly overexpressed in DUOC-01 cells relative to CD14⁺ cells. Some of these are listed in Supplemental File 2. In contrast, Supplemental File 2 shows that the list of genes more highly expressed in CB CD14⁺ cells is enriched in transcription factors and signaling molecules, particularly in repressors of transcription. Genes active in hematopoiesis and myeloid cell differentiation are also more common. Genes active in mitosis and cell cycle entry are much less common than in the list derived from DUOC-01.

We selected some of the transcripts overexpressed in DUOC-01 that are known to be important in promoting remyelination and confirmed their level of expression in CB CD14⁺ and DUOC-01 cells by quantitative PCR methods. Expression of these candidate molecules is presented in Table 1. Platelet-derived growth factor subunit A (*PDGFA*), KIT-ligand (*KITLG*, also known as stem cell factor [*SCF*]), insulin-like growth factor-1 (*IGF1*), triggering receptor expressed on myeloid cells 2 (*TREM2*), matrix metalloproteinase-9 (*MMP9*), and *MMP12* were highly upregulated in DUOC-01 cells compared with CB CD14⁺ monocytes; bioplex analysis also demonstrated that DUOC-1 cells secrete MMP9, MMP12, and other matrix proteases into culture supernatants (unpublished observation). *IL10* transcript levels were also enriched in DUOC-01 cells (Supplemental File 2), confirming our previous studies (20). Western blot analysis confirmed enrichment of TREM2, SCF, MMP9, and MMP12 proteins in DUOC-01 relative to CB CD14⁺ monocyte homogenates (Supplemental Figure 9). Higher expression of TREM2 on the DUOC-01 cell surface was also verified by flow cytometry (Supplemental Figure 9B). However, the relative abundance of IGF1 and PDGF-AA protein detected by Western blotting did not replicate transcript abundance (Supplemental Figure 9A). IGF1 and PDGF-AA proteins were detected in CD14⁺ CB monocytes but not in DUOC-01 homogenates. We hypothesized that our failure to detect IGF1 and PDGF-AA in DUOC-01 homogenates might result from their rapid secretion from the cells, as we have previously demonstrated that DUOC-01 cells secrete several proteins (20). To test this idea, DUOC-01 cells were allowed to adhere to glass slides and then incubated for 5 hours with brefeldin A (BFA). BFA treatment rapidly inhibits transport of secretory proteins from the ER to the Golgi, resulting in accumulation of proteins within the ER (48). Western blot analysis of DUOC-01 cells after BFA treatment showed higher intracellular concentrations of both IGF1 and PDGF-AA (Supplemental Figure 9C), indicating that these proteins are rapidly secreted by DUOC-01 cells. Immunocytochemical analysis of BFA-treated DUOC-01 cells using IGF1 and PDGF-AA antibodies also showed higher levels of staining after BFA treatment compared to cells without any BFA pretreatment (Supplemental Figure 9D). These data suggest that DUOC-01 cells express and secrete factors known to promote remyelination by several mechanisms and enhance oligodendrocyte precursor proliferation and differentiation.

Discussion

As we have discussed in detail elsewhere (20), the current NCT02254863 clinical trial using DUOC-01 to treat genetic metabolic diseases was predicated on the mechanistic assumption that intrathecally injected cell product can provide wild-type lysosomal enzyme replacement therapy to immunoablated CB transplant recipients. However, studies of the biological activities of DUOC-01 raised the possibility that the cell product has other types of potential benefits in treatment of demyelinating diseases (20). The studies presented here confirm that the DUOC-01 cell product strongly promotes remyelination in an animal model that does not depend on enzyme replacement: CPZ-induced demyelination of the CC. Injecting DUOC-01 cells into the CC area 1 day after CPZ-fed NSG mice were returned to normal diets dramatically accelerated reversal of all the pathological manifestations of CPZ feeding during the following week. The course of demyelination, astrogliosis, microgliosis, cellular accumulation, and the reversal of these processes following cessation of CPZ feeding in NSG mice closely resembled what has been reported in C57BL/6 mice (23, 25). Using CFSE-labeled DUOC-01 cells, we found that DUOC-01 cells reached brain regions remote from the injection site and that cells could be detected in the brain throughout the 1-week experiment. Storms et al. (49) have reported that a low percentage of intrathecally injected DUOC-01 cells persist in the brain of neonatal NSG mice for up to 56 days. Immunohistochemical and LFB-PAS staining demonstrated that DUOC-01 treatment accelerated remyelination of the CC, and electron microscopy revealed that administration of DUOC-01 cells increased the proportion of remyelinated axons and the thickness and organization of the myelin sheath following treatment. DUOC-01 treatment also significantly resolved gliosis in the CC induced by CPZ feeding. Finally, electron microscopic analysis also showed that DUOC-01 treatment reduced the number of megamitochondria in the CC region, suggesting that DUOC-01 treatment reverses metabolic stress (41, 50–52), abnormality of mitochondrial fission (53, 54), or oxidative stress induced by CPZ treatment. Thus, DUOC-01 cells can deploy within the cerebral cortex following intracerebral injection and accelerate remyelination after cessation of CPZ feeding. During manufacture of DUOC-01 from $CD14^+$ CB monocytes, expression of many factors that can influence remyelination by a variety of mechanisms is upregulated. These studies provide proof of concept for the clinical use of DUOC-01 in the treatment of demyelinating diseases.

Freshly isolated CB $CD14^+$ monocytes also accelerated remyelination and reduced cellular infiltration in the CC following discontinuation of CPZ feeding, but did so significantly less markedly than DUOC-01 cells. Because we are primarily interested in delineating the mechanism of action of the DUOC-01 cell product that is in the clinic, we have not studied the biodistribution or persistence of these cells following injection or performed detailed immunohistochemical or morphometric analysis of the effects of $CD14^+$ CB cells in the CPZ system. We do not know if both cell populations use the same mechanisms of action to accelerate remyelination. We note in this context that DUOC-01 treatment increased proliferation of oligodendrocyte lineage cells, but treatment with $CD14^+$ CB monocytes did not.

Our demonstration that CB $CD14^+$ monocytes are essential for the manufacture of DUOC-01 cells implies that changes in gene expression occurring during manufacturing enhance the ability of DUOC-01 cells to promote remyelination. Whole-genome expression analysis demonstrated that CB $CD14^+$ monocytes and DUOC-01 differed in their expression of thousands of transcripts, and subsequent studies based on real-time PCR, Western blotting, and flow cytometry confirmed that CB $CD14^+$ monocytes and DUOC-01 differ significantly in expression of some secretory proteins and other molecules that can promote remyelination following CPZ feeding by multiple mechanisms. While we used differences in gene expression between $CD14^+$ CB monocytes and DUOC-01 cell products as an initial screen to identify molecules that may play important mechanistic roles in accelerating remyelination, we note several caveats to this approach. First, transcript levels need not reflect levels of protein production. Indeed, we found that while both proteins and transcripts for SCF, TREM2, MMP9, and MMP12 were highly expressed in DUOC-01 but not expressed in $CD14^+$ CB monocytes, but IGF1 and PDGF-AA proteins were expressed in both cell types at similar levels in spite of differences in transcript levels. Second, some molecules that are expressed at similar levels by both cell types could play important roles in remyelination by both cell types; such molecules would not be detected if only differentially expressed transcripts were considered as candidates. Finally, we have not yet analyzed the changes in expression of transcripts when either DUOC-01 or $CD14^+$ CB monocytes are injected into brain tissue; the gene array data presented here only indicate what transcripts each cell population expressed at the time of treatment. The differentially expressed transcripts that we have detected provide markers for more in-depth analysis of

changes in injured tissue. Thus, the gene expression data provide a starting point to elucidate the mechanisms by which DUOC-01 promotes remyelination.

Several of the proteins that are expressed by DUOC-01 cells are known to regulate the number or activity of oligodendrocyte progenitor cells (OPCs). PDGFs regulate the OPC numbers in the adult CNS and their activity following CNS demyelination (55–57), and *PDGFA* transcript expression was upregulated 32-fold in the DUOC-01 compared with CB CD14$^+$ monocytes. SCF has been implicated in the maintenance, migration, and survival of the OPC population (58, 59), and its transcript was expressed at a 26-fold higher level in DUOC-01 cells than in CB CD14$^+$ cells. Similarly, expression of *IGF1* transcripts was almost 800-fold higher in DUOC-01 compared to the CD14$^+$ cells. IGF1 has been shown to induce myelination in vitro and in vivo and also protects mature oligodendrocytes from a pathological insult (34, 60, 61). Furthermore, IGF1 promotes the long-term survival of mature oligodendrocytes in culture and inhibits mature oligodendrocyte apoptosis in vitro (61, 62). Brefeldin A–mediated inhibition of secretory proteins demonstrated that PDGF-AA and IGF1 are both rapidly secreted from DUOC-01 cells. These factors, then, could directly drive the large increase in proliferating oligodendrocyte lineage cells that we observed in the CC of DUOC-01–treated animals compared with controls receiving no cell therapy.

TREM2 is another molecule expressed by DUOC-01 cells that may play an important role in remyelination. CD14$^+$ monocytes do not express TREM2 transcripts or protein. This surface receptor senses lipid debris and regulates signaling by glial cells that modulate myelination (63, 64). It also functions in clearance of cellular and myelin debris, an important early step for recovery and remyelination following CNS injury (12, 65). DUOC-01 cells are highly phagocytic (20) and could play a significant role in myelin clearance and intercellular signaling through the TREM2 receptor. DAVID analysis of differentially expressed genes showed that the lysosomal/intracellular vesicular pathway and Fcγ-mediated phagocytosis were among the most highly upregulated group of genes in DUOC-01 compared with CD14$^+$ CB monocytes (Supplemental File 2).

DUOC-01 cells express many other proteins that could participate more indirectly in promoting remyelination and in resolving cellular accumulation in the CC. Cytokine-activated microglia can stimulate the differentiation of oligodendrocytes from neural progenitor cells (66). While oligodendrocytes affect the remyelination of nerve fibers, other cell types are important for this repair process (33). Astrocytes provide trophic factors for oligodendrocytes and also for microglia (35). Microglia also provide trophic factors and remove myelin debris that inhibit remyelination by oligodendrocytes (11, 34, 36, 37). The microarray data indicate that several chemokines and other regulators of neuroinflammation are upregulated in DUOC-01 cells. We previously reported that DUOC-01 cells secrete IL-10 and TNF-α in culture (20). Yang et al. have demonstrated that neuronal stem cells producing IL-10 not only effectively suppress CNS inflammation but also promote remyelination and neuron/oligodendrocyte repopulation in a mouse model of experimental autoimmune encephalomyelitis (67). Furthermore, IL-10 promotes survival of neurons and oligodendrocytes by protecting them from inflammation-induced damage (68–70). It has been shown that TNF-α plays an important reparative role in the demyelinating brain. Lack of TNF-α led to a reduction in the pool of proliferating OPCs and subsequent significant delay in remyelination in CPZ-mediated demyelinated brain (71). The microarray data indicate that several other factors including chemokines and other regulators of neuroinflammation are upregulated in DUOC-01 cells.

DUOC-01 cells also overexpress proteases that can regulate remyelination through modification of the extracellular matrix. We confirmed upregulation of MMP9 and MMP12 by PCR and Western blotting. CD14$^+$ CB monocytes did not detectably express either protease. MMP9 activity is required to clear NG2 chondroitin sulfate proteoglycan deposition and overcome the negative impact of NG2 on oligodendrocyte maturation and remyelination (72). High expression of MMP12, which is required for proteolysis and matrix invasion by macrophages in mice, might facilitate the migration of DUOC-01 from the injection site in the CC to other regions of the brain that we observed using CFSE-labeled cells. MMPs also play a role in angiogenesis, in the release of growth factors sequestered by the extracellular matrix (73), and in processing of cell-cell recognition molecules that allow repair (74).

These studies constitute proof of concept that the monocyte-derived DUOC-01 cell product could provide benefit to patients with demyelinating conditions such as leukodystrophies, multiple sclerosis, or spinal cord injury. However, additional preclinical and early-phase clinical studies, based in part on the results presented here, will be necessary to bring this cell product to the clinic for treatment of such conditions. First, the route of administration, and resulting biodistribution of cell product, will need to be evaluated.

In the model presented in this report, we used intracerebral injection to maximize localization of cells adjacent to the injured area. This is a plausible, but not an optimal, route of clinical administration. Second, the question of whether there is persistence of cell product in an immune-competent patient will need to be explored. While this is not an issue in the studies presented here using immune-incompetent NSG mice or in the ongoing NCT02254863 clinical trial, as the patients are myelo- and immunoablated and the CB unit used for transplant is the same as the unit used to manufacture DUOC-01 (20), immunogenicity is likely to be important in other clinical settings. In the current clinical trial, systemic engraftment of the donor CB unit used to manufacture DUOC-01 must occur before DUOC-01 is administered intrathecally. Thus, the recipient is tolerized to the DUOC-01 donor. In other indications, systemic tolerization is unlikely to be included in the therapeutic approach, rather DUOC-01 will be administered as a stand-alone, partially HLA-matched, patient-directed cell therapy product. DUOC-01 is moderately immunogenic in mixed lymphocyte assays, although less so than peripheral blood MNCs (20), and the impact of this is not known but can be further explored in the CPZ model since we have found that the kinetics of de- and remyelination appear to be the same in immune-competent and NSG animals. Also, the gene expression data presented here provide the basis for continuing studies of the mechanism of action of the DUOC-01 cell product and assays of product potency and release. The biological activity of DUOC-01 reported here suggests that it has potential for the treatment of disorders of myelination in the clinic and that these preclinical studies should be considered as part of the clinical development program of this interesting and potentially novel CB-derived cell therapy product.

Methods

Animals and animal welfare. Male NSG mice (NOD/SCID/IL2Rγ^{null}) were supplied by NSG Breeding Core of Duke Division of Laboratory Animal Resources and were maintained under specific pathogen–free conditions.

Manufacture of DUOC-01. DUOC-01 cells were prepared from cryopreserved CB units and formulated in Ringer's solution using the protocols developed to make products for clinical use (20). These methods have been described in detail (20). For convenience, this material is reproduced in the Supplemental Materials.

Separation of specific cell populations from CB. $CD14^+$ populations from cryopreserved CB were immunomagnetically selected using Whole Blood CD14 Microbeads as described by the manufacturer (Miltenyi Biotec). Cells that did not adhere to the anti-CD14 antibody columns comprised the $CD14^+$-depleted population. Some experiments were carried out with cells from $CD14^+$ cells from freshly collected CB. MNC populations depleted of erythrocytes were prepared from fresh CB either by centrifugation on Ficoll or in SepMate tubes (STEMCELL Technologies) as described by the manufacturer. $CD14^+$ cells were immunomagnetically purified from MNC preparations using the CD14 Microbeads. Similar experiments were carried out with CB cell populations enriched for or depleted of CD34-expressing cells using anti-CD34 Microbeads (Miltenyi Biotec).

To prepare $CD14^+$ cell RNA for microarray analysis, freshly collected CB was centrifuged on Ficoll to prepare MNC fractions. These fractions were treated with 0.15 M NH_4Cl to lyse erythrocytes, washed in PBS, and then incubated on ice with PeCy7-mouse anti–human CD14 (catalog 562698), FITC-mouse anti–human CD3 (catalog 555339), and FITC-mouse anti–human CD235a (catalog 559943) antibodies (all from BD). Cells were then sorted twice by flow cytometry to yield $CD14^+CD235a^-CD3^-$ populations. The first enrichment sort was followed by a second purity sort. Cells were maintained at 0°C–4°C during all procedures, including flow sorting. The purity of selected populations and the extent of $CD14^+$ cell depletion were determined by flow cytometry as previously described (20).

CPZ demyelination in NSG mice. Eight-week-old male NSG mice were acclimated to milled standard rodent chow for 1 week. Demyelination was subsequently induced by incorporating 0.2% by weight CPZ (bis-cyclohexanone oxaldihydrazone, Sigma-Aldrich) into the milled chow for 5 weeks. Brains were then harvested from CPZ-fed animals and controls were fed chow without CPZ for subsequent assessment of the degree of demyelination and disruption of brain histology induced by CPZ. To assess the effects of cell treatment, 2 additional groups of animals were returned to standard diet to allow remyelination. One day after the change in diet, animals were stereotactically injected in the CC (coordinates: 0.2 mm posterior and 1.1 mm lateral to the bregma, and 1.5 mm deep from the skull surface) with 10^5 cells (DUOC-01 or $CD14^+$) in 5 μl of lactated Ringer's solution or with excipient within the 2-hour expiry period for the DUOC-01 clinical cell product. One week following treatment, brains were harvested by intracardiac perfusion with

PBS and then with 4% paraformaldehyde. Paraffin-embedded coronal sections were prepared for analysis of myelination status, the organization of neural fibers, and persistence of injected human cells by LFB-PAS staining, immunohistochemistry, and electron microscopy as described below. Cohorts of 5 or 6 mice were analyzed under each set of experimental conditions.

Myelination, cellular infiltration, and gliosis were assessed by LFB-PAS staining of the CC region, (approximately at the level of the bregma –0.2 to –0.9 mm) (75). We used 5.0-μm-thick paraffin-embedded coronal sections of the CC region. LFB stains the myelin blue, and PAS stains demyelinated axons pink. Three independent, blinded readers scored coded LFB-PAS–stained sections between 0 and 3. A score of 3 is equivalent to the myelin status of a brain not treated with CPZ; 0 is equivalent to a completely demyelinated brain area. A score of 1 or 2 corresponds to one-third or two-third fiber myelination, respectively. Similarly, a quantitative cellularity score was obtained by counting the number of nuclei in the CC region of LFB-stained brain slices on a scale of 0 to 3, by blinded readers.

Immunohistochemistry. Detailed protocols are presented in the Supplemental Methods. Brain slices from 3 animals in each treatment group were analyzed. Primary antibodies used were: rat anti-MBP (1:1,000, Abcam, catalog ab7349); chicken anti-NFH (1:100,000, EnCor Biotech, catalog CPCA-NF-H); mouse anti-HuN (1:250, Millipore, catalog MAB1281); chicken anti-GFAP (1:500, Abcam, catalog ab4674); goat anti-Iba1 (1:200, Abcam, catalog ab5076); rabbit anti-Ki67 (1:300, Abcam, catalog ab15580); and goat anti-Olig2 (1:50, R&D Systems, catalog AF2418). Secondary antibodies used were: Alexa-488 donkey anti-rat, Alexa-647 donkey anti-chicken, Alexa-568 donkey anti-mouse (1:500, Molecular Probes). Confocal micrographs were obtained using constant settings including laser power, stack thickness, and camera resolution. The number of stained cells per microscopic field in the CC region and the average area covered by cells stained with each antibody were quantified by ImageJ software (NIH).

Electron microscopy. Preparation of brains for electron microscopy is described in detail in the Supplemental Methods. Images were then analyzed using ImageJ software. For analysis, g-ratio analysis was modified such that the inner diameter of compact myelin (instead of the axon diameter) was divided by the outer diameter of the myelin sheath. Diameters were calculated from enclosed areas. Fibers with prominent outfoldings in the plane of section were excluded. We implemented a plugin for the ImageJ software (http://rsbweb.nih.gov/ij), which allowed for semiautomated analysis of randomly selected sets of fibers (76). Plugin and source code are available online (http://gratio.efil.de). A minimum of 100 fibers/mouse, 3 mice/time point/treatment, were analyzed. The number of mitochondria in all cells in the CC area was counted in all the electron micrographs, and average mitochondria present per ×8,800-magnified field was calculated. To determine the size of the mitochondria, electron microscopic images were analyzed with ImageJ, using the area analysis function. For area measurement, the mitochondria were circled by the lasso tool, and then the areas of the circles were calculated and converted to their actual values using the scale bar. At least 10 images were analyzed per sample in a blinded fashion.

Tracking DUOC-01 cells in the brain. DUOC-01 cells were stained with 5 μM Vybrant CFDA SE Cell Tracer dye (CFSE, V12883, green fluorescence, Life Technologies) and injected into the CC as described above. One, four, and seven days later, brains were harvested, sliced, and processed for confocal microscopy.

Expression analysis by microarrays. RNA for microarray analysis was prepared from 4 flow-sorted $CD14^+$ CB and 3 DUOC-01 products using the QIAGEN RNeasy Mini Kit as described by the manufacturer. These samples were used for whole-genome microarray analysis on 1 chip. Microarray analysis was performed by the Microarray Shared Resource in the Duke Center for Genomic and Computational Biology using Affymetrix GeneChip Human Transcriptome Array 2.0 microarrays. Partek Genomics Suite 6.6 (Partek Inc.) was used to perform data analysis. Robust multichip analysis (RMA) normalization was performed on the entire dataset. Multi-way ANOVA and analysis of the fold change were performed to select target genes that were differentially expressed. Hierarchical clustering was performed on differentially expressed genes based on average linkage with Pearson's dissimilarity.

RNA isolation and quantitative real-time PCR. Quantitative real-time RT-PCR was used to measure levels of transcripts in $CD14^+$ CB cells, DUOC-01, and cell products manufactured from isolated $CD14^+$ CB cells using the RNeasy Mini Kit with DNAse-1 treatment as instructed. The cDNA was synthesized from equal amounts of RNA using SuperScript III enzyme, oligo(dT) primers, dNTPs, RNase Out, DTT, and buffer as instructed (Life Technologies). Diluted cDNA was amplified on the Bio-Rad CFX96 Real Time System using SsoAdvanced Universal SYBR Green Supermix (Bio-Rad) and the following oligonucleotides: *PDGFA* (sense 5′-CTTCCTCGATGCTTCTCTTCC-3′, antisense 5′-GACCTCCAGCGACTCCT-3′); *MMP9*

(sense 5′-TGTACCGCTATGGTTACACTCG-3′, antisense 5′- GGCAGGGACAGTTGCTTCT-3′); *IGF1* (sense 5′-GCCTCCTTAGATCACAGCTC-3′, antisense 5′-GATGCTCTTCAGTTCGTGTGT-3′); *IL10* (sense 5′-GCGCTGTCATCGATTTCTTC-3′, antisense 5′-TCACTCATGGCTTTGTAGATGC-3′); *MMP12* (sense 5′-CAAAACTCAAATTGGGGTCACAG-3′, antisense 5′-CTCTCTGCTGATGACATACGTG-3′), *KITLG* (sense 5′-AGCTGAAGATAAATGCAAGTGAG-3′, antisense 5′-CAGAACAGCTAAACGGAGTCG-3′), and *TREM2* (sense 5′-TCATAGGGGCAAGACACCT-3′, antisense 5′-GCTGCTCATCTTACTCTTTGTC-3′). Values were normalized to *GAPDH* expression.

Statistics. In most cases statistical comparisons were conducted with 2-tailed Student's *t* tests with unequal variance. For comparing LFB and cellularity scores we used Wilcoxon rank-sum tests. Statistical comparisons were performed using the Wilcoxon rank-sum test for clustered data using the *clusrank* package in R. Mean differences were considered significant if *P* values were less than 0.05.

Study approval. All animal experimentation protocols were approved by the Duke University IACUC and were conducted in accordance with the United States Public Health Service Policy on Human Care and Use of Laboratory Animals.

Author contributions

All authors reviewed the manuscript. In addition, JK conceived and directed the DUOC-01 development program and edited the manuscript; AEB designed and directed the research, analyzed data, and edited the manuscript; AS designed, directed, and performed experiments, and drafted the manuscript; SB managed the research, performed experiments, and analyzed the data; LX, PS, PN, AW, SP, and AG performed experiments; GM advised on CPZ experiments, analyzed related data, and critically reviewed the manuscript; TG developed and directed cGMP manufacturing and designed experiments.

Acknowledgments

The authors are grateful to the staff at the Carolinas Cord Blood Bank for providing cord blood units for the experiments described, Lynn Cheatham for help with graphics, Marcia Bentz and Roderick Franczak for helping in tissue preparation and staining, Neil Medvitz of Duke Pathology for performing electron microscopy, April Ozamiz, Benjamin Rusche, Norin Meadows, and Frankie Shaw of the GMP lab for helping with DUOC-01 cells preparation, David Snyder of Department of Surgery for IC injections, Michael Cook at the Duke Cancer Institute Core Flow Cytometry Facility for assistance with cell sorting, Zhengzheng Wei at the Duke Institute for Genomic Sciences Microarray Core Facility for performing and helping analyze microarray data, and to Benjamin Carlson at the Light Microscopy Core Facility at Duke University for assistance with image analysis. Amy Wollish was supported by a National Cancer Institute of the National Institutes of Health Award (grant 5T32CA074736, Research Training in Neuro-Oncology). This work was supported by the Julian Robertson Foundation and by the Marcus Foundation.

Address correspondence to: Arjun Saha, Room 0104, Research Park 2, PO Box 103455, Robertson Clinical and Translational Cell Therapy Program, Duke Translational Medicine Institute, Duke University Medical Center, Durham, North Carolina 27710, USA. Phone: 919.684.3934; E-mail:arjun.saha@duke.edu.

AW's present address is: PPD Inc., Wilmington, North Carolina, USA.

1. Nayak D, Roth TL, McGavern DB. Microglia development and function. *Annu Rev Immunol*. 2014;32:367–402.
2. Ginhoux F, Lim S, Hoeffel G, Low D, Huber T. Origin and differentiation of microglia. *Front Cell Neurosci*. 2013;7:45.
3. Matsushima GK, et al. Absence of MHC class II molecules reduces CNS demyelination, microglial/macrophage infiltration, and twitching in murine globoid cell leukodystrophy. *Cell*. 1994;78(4):645–656.
4. Louveau A, et al. Structural and functional features of central nervous system lymphatic vessels. *Nature*. 2015;523(7560):337–341.
5. Ginhoux F, et al. Fate mapping analysis reveals that adult microglia derive from primitive macrophages. *Science*. 2010;330(6005):841–845.
6. Mildner A, et al. Microglia in the adult brain arise from Ly-6C^{hi}CCR2^{+} monocytes only under defined host conditions. *Nat Neurosci*. 2007;10(12):1544–1553.
7. Lampron A, Pimentel-Coelho PM, Rivest S. Migration of bone marrow-derived cells into the central nervous system in models of neurodegeneration. *J Comp Neurol*. 2013;521(17):3863–3876.
8. McMahon EJ, Suzuki K, Matsushima GK. Peripheral macrophage recruitment in cuprizone-induced CNS demyelination despite an intact blood-brain barrier. *J Neuroimmunol*. 2002;130(1–2):32–45.
9. Wohleb ES, McKim DB, Sheridan JF, Godbout JP. Monocyte trafficking to the brain with stress and inflammation: a novel axis

of immune-to-brain communication that influences mood and behavior. *Front Neurosci*. 2014;8:447.
10. Reader BF, Jarrett BL, McKim DB, Wohleb ES, Godbout JP, Sheridan JF. Peripheral and central effects of repeated social defeat stress: monocyte trafficking, microglial activation, and anxiety. *Neuroscience*. 2015;289:429–442.
11. Miron VE, Franklin RJ. Macrophages and CNS remyelination. *J Neurochem*. 2014;130(2):165–171.
12. Lampron A, et al. Inefficient clearance of myelin debris by microglia impairs remyelinating processes. *J Exp Med*. 2015;212(4):481–495.
13. Shechter R, et al. Recruitment of beneficial M2 macrophages to injured spinal cord is orchestrated by remote brain choroid plexus. *Immunity*. 2013;38(3):555–569.
14. Ruckh JM, et al. Rejuvenation of regeneration in the aging central nervous system. *Cell Stem Cell*. 2012;10(1):96–103.
15. Shi C, Pamer EG. Monocyte recruitment during infection and inflammation. *Nat Rev Immunol*. 2011;11(11):762–774.
16. Shechter R, Schwartz M. Harnessing monocyte-derived macrophages to control central nervous system pathologies: no longer 'if' but 'how'. *J Pathol*. 2013;229(2):332–346.
17. Sanberg PR, et al. Monocyte transplantation for neural and cardiovascular ischemia repair. *J Cell Mol Med*. 2010;14(3):553–563.
18. Sun JM, Kurtzberg J. Cord blood for brain injury. *Cytotherapy*. 2015;17(6):775–785.
19. Womble TA, et al. Monocytes are essential for the neuroprotective effect of human cord blood cells following middle cerebral artery occlusion in rat. *Mol Cell Neurosci*. 2014;59:76–84.
20. Kurtzberg J, et al. Preclinical characterization of DUOC-01, a cell therapy product derived from banked umbilical cord blood for use as an adjuvant to umbilical cord blood transplantation for treatment of inherited metabolic diseases. *Cytotherapy*. 2015;17(6):803–815.
21. Zendedel A, Beyer C, Kipp M. Cuprizone-induced demyelination as a tool to study remyelination and axonal protection. *J Mol Neurosci*. 2013;51(2):567–572.
22. Skripuletz T, Gudi V, Hackstette D, Stangel M. De- and remyelination in the CNS white and grey matter induced by cuprizone: the old, the new, and the unexpected. *Histol Histopathol*. 2011;26(12):1585–1597.
23. Kipp M, Clarner T, Dang J, Copray S, Beyer C. The cuprizone animal model: new insights into an old story. *Acta Neuropathol*. 2009;118(6):723–736.
24. Torkildsen O, Brunborg LA, Myhr KM, Bø L. The cuprizone model for demyelination. *Acta Neurol Scand, Suppl*. 2008;188:72–76.
25. Matsushima GK, Morell P. The neurotoxicant, cuprizone, as a model to study demyelination and remyelination in the central nervous system. *Brain Pathol*. 2001;11(1):107–116.
26. Bénardais K, et al. Cuprizone [bis(cyclohexylidenehydrazide)] is selectively toxic for mature oligodendrocytes. *Neurotox Res*. 2013;24(2):244–250.
27. Einstein O, Friedman-Levi Y, Grigoriadis N, Ben-Hur T. Transplanted neural precursors enhance host brain-derived myelin regeneration. *J Neurosci*. 2009;29(50):15694–15702.
28. Crocker SJ, et al. Intravenous administration of human embryonic stem cell-derived neural precursor cells attenuates cuprizone-induced central nervous system (CNS) demyelination. *Neuropathol Appl Neurobiol*. 2011;37(6):643–653.
29. Hedayatpour A, et al. Promotion of remyelination by adipose mesenchymal stem cell transplantation in a cuprizone model of multiple sclerosis. *Cell J*. 2013;15(2):142–151.
30. Nessler J, et al. Effects of murine and human bone marrow-derived mesenchymal stem cells on cuprizone induced demyelination. *PLoS One*. 2013;8(7):e69795.
31. Arnett HA, et al. bHLH transcription factor Olig1 is required to repair demyelinated lesions in the CNS. *Science*. 2004;306(5704):2111–2115.
32. Mason JL, et al. Oligodendrocytes and progenitors become progressively depleted within chronically demyelinated lesions. *Am J Pathol*. 2004;164(5):1673–1682.
33. Gudi V, Gingele S, Skripuletz T, Stangel M. Glial response during cuprizone-induced de- and remyelination in the CNS: lessons learned. *Front Cell Neurosci*. 2014;8:73.
34. Mason JL, Ye P, Suzuki K, D'Ercole AJ, Matsushima GK. Insulin-like growth factor-1 inhibits mature oligodendrocyte apoptosis during primary demyelination. *J Neurosci*. 2000;20(15):5703–5708.
35. Biancotti JC, Kumar S, de Vellis J. Activation of inflammatory response by a combination of growth factors in cuprizone-induced demyelinated brain leads to myelin repair. *Neurochem Res*. 2008;33(12):2615–2628.
36. Skripuletz T, et al. Astrocytes regulate myelin clearance through recruitment of microglia during cuprizone-induced demyelination. *Brain*. 2013;136(Pt 1):147–167.
37. Clarner T, et al. Myelin debris regulates inflammatory responses in an experimental demyelination animal model and multiple sclerosis lesions. *Glia*. 2012;60(10):1468–1480.
38. Hiremath MM, Saito Y, Knapp GW, Ting JP, Suzuki K, Matsushima GK. Microglial/macrophage accumulation during cuprizone-induced demyelination in C57BL/6 mice. *J Neuroimmunol*. 1998;92(1–2):38–49.
39. Hibbits N, Yoshino J, Le TQ, Armstrong RC. Astrogliosis during acute and chronic cuprizone demyelination and implications for remyelination. *ASN Neuro*. 2012;4(6):393–408.
40. Shultz LD, et al. Human lymphoid and myeloid cell development in NOD/LtSz-scid IL2R gamma null mice engrafted with mobilized human hemopoietic stem cells. *J Immunol*. 2005;174(10):6477–6489.
41. Praet J, Guglielmetti C, Berneman Z, Van der Linden A, Ponsaerts P. Cellular and molecular neuropathology of the cuprizone mouse model: clinical relevance for multiple sclerosis. *Neurosci Biobehav Rev*. 2014;47:485–505.
42. Karrer FM, Reitz BL, Hao L, Lafferty KJ. Fluorescein labeling of murine hepatocytes for identification after intrahepatic transplantation. *Transplant Proc*. 1992;24(6):2820–2821.
43. Dimou L, Simon C, Kirchhoff F, Takebayashi H, Götz M. Progeny of Olig2-expressing progenitors in the gray and white matter of the adult mouse cerebral cortex. *J Neurosci*. 2008;28(41):10434–10442.
44. Fancy SP, Chan JR, Baranzini SE, Franklin RJ, Rowitch DH. Myelin regeneration: a recapitulation of development? *Annu Rev Neurosci*. 2011;34:21–43.
45. Scholzen T, Gerdes J. The Ki-67 protein: from the known and the unknown. *J Cell Physiol*. 2000;182(3):311–322.
46. Huang da W, Sherman BT, Lempicki RA. Systematic and integrative analysis of large gene lists using DAVID bioinformatics

resources. *Nat Protoc*. 2009;4(1):44–57.
47. Huang da W, Sherman BT, Lempicki RA. Bioinformatics enrichment tools: paths toward the comprehensive functional analysis of large gene lists. *Nucleic Acids Res*. 2009;37(1):1–13.
48. Misumi Y, Misumi Y, Miki K, Takatsuki A, Tamura G, Ikehara Y. Novel blockade by brefeldin A of intracellular transport of secretory proteins in cultured rat hepatocytes. *J Biol Chem*. 1986;261(24):11398–11403.
49. Storms R, et al. Tissue distribution of a cord blood-derived cell product following intrathecal transplantation. *Cytotherapy*. 2014;16(4):S63.
50. Kashani IR, et al. Protective effects of melatonin against mitochondrial injury in a mouse model of multiple sclerosis. *Exp Brain Res*. 2014;232(9):2835–2846.
51. Tandler B, Hoppel CL. Division of giant mitochondria during recovery from cuprizone intoxication. *J Cell Biol*. 1973;56(1):266–272.
52. Acs P, Komoly S. Selective ultrastructural vulnerability in the cuprizone-induced experimental demyelination. *Ideggyogy Sz*. 2012;65(7–8):266–270.
53. Flatmark T, Kryvi H, Tangerås A. Induction of megamitochondria by cuprizone(biscyclohexanone oxaldihydrazone). Evidence for an inhibition of the mitochondrial division process. *Eur J Cell Biol*. 1980;23(1):141–148.
54. Asano M, Wakabayashi T, Ishikawa K, Kishimoto H. Mechanism of the formation of megamitochondria by copper-chelating agents. IV. Role of fusion phenomenon in the cuprizone-induced megamitochondrial formation. *Acta Pathol Jpn*. 1978;28(2):205–213.
55. Woodruff RH, Fruttiger M, Richardson WD, Franklin RJ. Platelet-derived growth factor regulates oligodendrocyte progenitor numbers in adult CNS and their response following CNS demyelination. *Mol Cell Neurosci*. 2004;25(2):252–262.
56. Murtie JC, Zhou YX, Le TQ, Vana AC, Armstrong RC. PDGF and FGF2 pathways regulate distinct oligodendrocyte lineage responses in experimental demyelination with spontaneous remyelination. *Neurobiol Dis*. 2005;19(1–2):171–182.
57. Vana AC, Flint NC, Harwood NE, Le TQ, Fruttiger M, Armstrong RC. Platelet-derived growth factor promotes repair of chronically demyelinated white matter. *J Neuropathol Exp Neurol*. 2007;66(11):975–988.
58. Ida JA, Dubois-Dalcq M, McKinnon RD. Expression of the receptor tyrosine kinase c-kit in oligodendrocyte progenitor cells. *J Neurosci Res*. 1993;36(5):596–606.
59. Erlandsson A, Larsson J, Forsberg-Nilsson K. Stem cell factor is a chemoattractant and a survival factor for CNS stem cells. *Exp Cell Res*. 2004;301(2):201–210.
60. D'Ercole AJ, Ye P, Calikoglu AS, Gutierrez-Ospina G. The role of the insulin-like growth factors in the central nervous system. *Mol Neurobiol*. 1996;13(3):227–255.
61. García-Segura LM, et al. Interaction of the signalling pathways of insulin-like growth factor-I and sex steroids in the neuroendocrine hypothalamus. *Horm Res*. 1996;46(4–5):160–164.
62. Cho KH, Kim MW, Kim SU. Tissue culture model of Krabbe's disease: psychosine cytotoxicity in rat oligodendrocyte culture. *Dev Neurosci*. 1997;19(4):321–327.
63. Wang Y, et al. TREM2 lipid sensing sustains the microglial response in an Alzheimer's disease model. *Cell*. 2015;160(6):1061–1071.
64. Cantoni C, et al. TREM2 regulates microglial cell activation in response to demyelination in vivo. *Acta Neuropathol*. 2015;129(3):429–447.
65. Tsiperson V, Li X, Schwartz GJ, Raine CS, Shafit-Zagardo B. GAS6 enhances repair following cuprizone-induced demyelination. *PLoS One*. 2010;5(12):e15748.
66. Butovsky O, et al. Microglia activated by IL-4 or IFN-gamma differentially induce neurogenesis and oligodendrogenesis from adult stem/progenitor cells. *Mol Cell Neurosci*. 2006;31(1):149–160.
67. Yang J, et al. Adult neural stem cells expressing IL-10 confer potent immunomodulation and remyelination in experimental autoimmune encephalitis. *J Clin Invest*. 2009;119(12):3678–3691.
68. Strle K, et al. Interleukin-10 in the brain. *Crit Rev Immunol*. 2001;21(5):427–449.
69. Molina-Holgado F, Grencis R, Rothwell NJ. Actions of exogenous and endogenous IL-10 on glial responses to bacterial LPS/cytokines. *Glia*. 2001;33(2):97–106.
70. Boyd ZS, Kriatchko A, Yang J, Agarwal N, Wax MB, Patil RV. Interleukin-10 receptor signaling through STAT-3 regulates the apoptosis of retinal ganglion cells in response to stress. *Invest Ophthalmol Vis Sci*. 2003;44(12):5206–5211.
71. Arnett HA, Mason J, Marino M, Suzuki K, Matsushima GK, Ting JP. TNF alpha promotes proliferation of oligodendrocyte progenitors and remyelination. *Nat Neurosci*. 2001;4(11):1116–1122.
72. Larsen PH, Wells JE, Stallcup WB, Opdenakker G, Yong VW. Matrix metalloproteinase-9 facilitates remyelination in part by processing the inhibitory NG2 proteoglycan. *J Neurosci*. 2003;23(35):11127–11135.
73. Whitelock JM, Murdoch AD, Iozzo RV, Underwood PA. The degradation of human endothelial cell-derived perlecan and release of bound basic fibroblast growth factor by stromelysin, collagenase, plasmin, and heparanases. *J Biol Chem*. 1996;271(17):10079–10086.
74. Yong VW, Power C, Forsyth P, Edwards DR. Metalloproteinases in biology and pathology of the nervous system. *Nat Rev Neurosci*. 2001;2(7):502–511.
75. Doan V, Kleindienst AM, McMahon EJ, Long BR, Matsushima GK, Taylor LC. Abbreviated exposure to cuprizone is sufficient to induce demyelination and oligodendrocyte loss. *J Neurosci Res*. 2013;91(3):363–373.
76. Goebbels S, et al. Elevated phosphatidylinositol 3,4,5-trisphosphate in glia triggers cell-autonomous membrane wrapping and myelination. *J Neurosci*. 2010;30(26):8953–8964.